C. R. Mecanique 343 (2015) 264–274

Contents lists available at ScienceDirect

Comptes Rendus Mecanique

www.sciencedirect.com

A porous model to simulate the evolution of the soil–water characteristic curve with volumetric strains

Hiram Arroyo [a,*], Eduardo Rojas [a], María de la Luz Pérez-Rea [a], Jaime Horta [a], José Arroyo [b]

[a] Faculty of Engineering, Universidad Autónoma de Querétaro, Centro Universitario, Cerro de las Campanas, 76160, Querétaro, Qro., Mexico
[b] Faculty of Civil Engineering, Universidad Michoacana de San Nicolás de Hidalgo, Centro Universitario, Avenida Francisco J. Mújica S/N, 58030, Morelia, Mich., Mexico

ARTICLE INFO

Article history:
Received 2 October 2014
Accepted 3 February 2015
Available online 20 February 2015

Keywords:
Unsaturated soils
Retention curve
Hysteresis
Constitutive modeling
Geotechnical models

ABSTRACT

Volumetric strains modify the soil–water retention curve. An easy way to take this phenomenon into account is by means of a percolation model based on the pore size distribution of the material. The model proposed herein is able to simulate the retention curves during wetting–drying cycles. As volumetric deformations modify the pore size distribution, its effect on the retention curves can be easily included in the model. The model is validated by comparing some numerical results with experimental results. This procedure represents an option to create fully coupled constitutive models for unsaturated soils.

1. Introduction

It has been well documented that mechanical and hydraulic behavior in unsaturated soils are coupled. An unsaturated soil is a multiphase medium that contains at least three interacting phases. These interactions induce a negative pore water pressure that bonds solid particles to each other. Resistance and volumetric strains depend very much on these water bonds [1]. When water menisci are formed between concurrent solid particles, an additional contact stress appears, bringing them closer and shrinking the porous structure of the material. If suction reduces, two different behaviors may occur. If the soil mass is not loaded further previous to wetting, the volume of the soil suffers an elastic rebound. On the contrary, if the soil is loaded beyond the yield surface previous to wetting, the porous structure of the soil collapses. This volumetric reduction influences the hydraulic behavior of the material.

It is therefore important to understand the relationship between the amount of water in the soil with its corresponding suction. From the point of view of constitutive modeling, it is more important to determine the degree of saturation Sr—the ratio between water volume and volume of voids—because suction and the strain-like variable nSr are both conjugate variables of the soil–air–water system, n being the soil porosity of the material [2,3]. Once plotted in a Cartesian coordinate system, the relationship s–Sr is called soil–water retention curve or soil–water characteristic curve [SWCC]. In addition, suction (s) can be related to the relative humidity of the medium through Kelvin's equation, or to the size of pores through Laplace's equation ($s = 2Ts/R$), where R represents the radius of the pore and Ts is the air–water interface tension coefficient.

* Corresponding author. Tel.: +52 442 192 1200x6031; fax: +52 442 192 1200x6005.
E-mail address: hiramarroyo@hotmail.com (H. Arroyo).

http://dx.doi.org/10.1016/j.crme.2015.02.001
1631-0721/

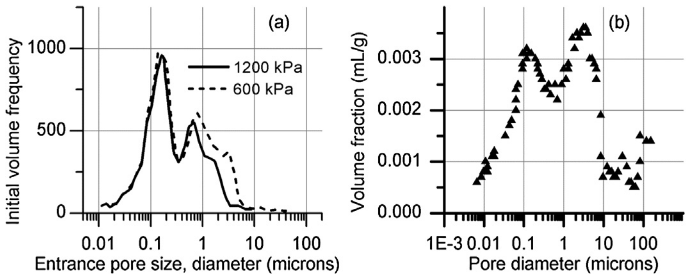

Fig. 1. (a) Comparing intrusion volume frequency ratios of samples compacted at the same water content and different vertical stresses [18], (b) pore-size distributions (PSD) of a clayey till subjected to 840 kPa of suction [19].

Despite its importance, prediction of SWCCs is a complicated task because they are highly dependent on the drying–wetting path. Hence, predictions on SWCCs that include the influence of volumetric deformations are difficult, as it is rather hard to predict how the overall soil structure modifies itself with suction or external stresses. However, this task cannot be avoided when modeling unsaturated soils.

Because internal pore structure and SWCCs are intimately related, there have been some attempts at simulating the hydraulic behavior of soils through equations that introduce some parameters that depend on the pore–size distribution (PSD). Based on Brooks and Corey's equation [4], Khalili [5] proposed a coupled hydromechanical model where the shifting of the SWCCs along the suction axis is a function of the air-entry value. Many models [6–9] modify van Genutchen's equation [10] by incorporating functions that depend on the current void ratio. In that sense, Romero and Vaunat [8] and later Vaunat [9] incorporated the influence of volume changes on the SWCC by quantifying the volume of micropores.

An interesting solution to model internal structural changes has been presented by Koliji et al. [11] who proposed a model to reproduce the evolution of the PSDs during suction increase or loading. Their study is based on experimental observations of PSDs obtained from samples subjected to different suctions. The PSD was obtained from mercury intrusion porosimetry (MIP) tests performed before and after the increment of suction. If this procedure is adapted to a porous model able to reproduce the SWCCs, then it is possible to include the effect of suction or loading on the shifting of the SWCCs. A model of this type is presented herein.

This paper presents a model that has been successfully used to reproduce the PSD of soils from the SWCCs and to correctly interpret the results of MIP tests [12,13]. This model is enhanced to couple volume change and water retention properties focusing on hydraulic hysteresis by proposing a simple yet effective way to simulate the evolution of the PSD.

2. Microstructural volume change

The sizes of pores in soil samples may range between thousandths to hundreds of microns. Coarse clean sands show relatively large pores of uniform size. In comparison, clay particles attract each other by electrochemical forces forming aggregates. This is why clayey soils generally show a double structure with small pores inside the aggregates (intrapores) and large pores between the aggregates (interpores) [14]. This type of structure can be observed through the results of MIP tests performed on these materials. As experimentally demonstrated by Simms and Yanful [15] and later by Romero et al. [16], the PSD modifies during loading or suction increase. Cuisinier and Laloui [17] observed strong modifications of the soil fabric with suction variations.

Fig. 1 shows the variations of volume with the size of pores of a glacial deposit best known as glacial till corresponding to unsorted materials with no apparent stratification commonly including fine grained components such as clay [20]. Notice that both Figs. 1a and 1b clearly show two maximum peaks exhibiting two main structural levels: micro and macroporosity. Here, the pores belonging to the larger sizes are called macropores (denoted by M) and those of smaller sizes are called micropores (denoted by mS site).

Fig. 2 shows the PSD of a soil sample subjected to different values of suction including the saturated conditions ($s = 0$). In this figure, the vertical axis represents the ratio of the volume of injected mercury with the logarithm of the pore radius r, while the horizontal axis represents the pore radius r in logarithmic scale. This figure indicates the contribution of each size to the total volume of pores. The nil suction curve shows a peak at a pore size of about 5 microns (macroporosity). As suction increases, macropores reduce their volume and the peak displaces to a smaller pore size of about 0.45 microns (microporosity). In other words, while the volume of macropores reduces, that of micropores increases.

As aforementioned, suction reduction (wetting) may induce expansion or collapse of the soil structure. Consider a soil subjected to certain suction level. In that case, solid particles are linked by water menisci that induce additional contact forces to these particles. When the soil is soaked, water menisci are destroyed and a general elastic rebound of the material is observed.

Collapse has been frequently related to silty sands subjected to loading while suction is present [21,22]. In this case, relatively large soil grains (sands) are linked by small packets of silt and clay (Fig. 3) which maintain larger grains practically immobile [21,23] when the soil is subjected to further loading. Because the strength of the packets depends on the amount

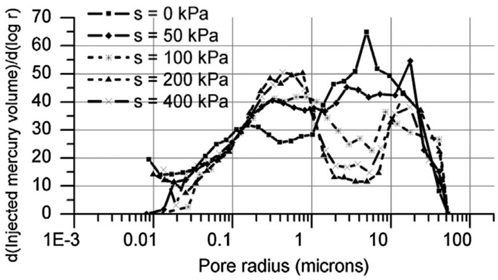

Fig. 2. Modification of samples fabric when suction is increased from 0 up to 400 kPa [17].

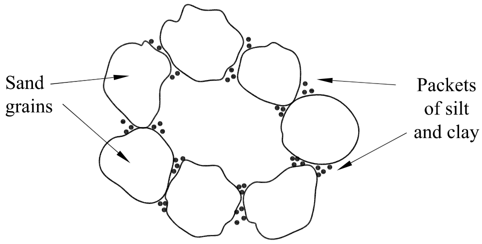

Fig. 3. Structural arrangement of collapsible soils.

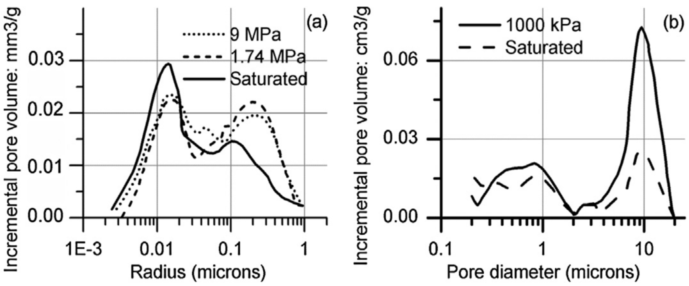

Fig. 4. Evolution of the PSD during wetting: (a) 70–30% Kunigel clay/Hostun sand mixture [24], (b) speswhite kaolin clay [25].

of water, when the volume of water is increased in the sample, the whole structure collapses, inducing plastic volumetric strains. The amount of collapse depends on the level of external loads.

From an elastoplastic point of view, elastic deformations during wetting or unloading do not generate important changes in the PSD of the soil. However, plastic deformations during collapse and virgin loading generate an irreversible change in the PSD due to the shrinking of macropores.

From the analyses of the experimental results shown in Figs. 1, 2 and 4, it can be said that the evolution of the PSD shows a reduction of the relative volume of macropores while that of micropores increases (see Figs. 1a, 2 and 4a). Notice however that, the general shape of the distribution of macropores remains practically unchanged. Because volumetric deformation is largely due to the shrinkage of macropores [19] and in order to keep the modeling as simple as possible, it is considered here that macropores in general shrink to smaller sizes. This type of behavior can be easily introduced in a porous model to simulate the evolution of the SWCCs with volumetric deformation.

3. Model formulation

3.1. Network construction

The two-dimensional porous model presented here includes two types of entities: the sites and the bonds. The sites or cavities are the larger pores that contain most of the volume of pores (see Fig. 5) and they are linked by the bonds. The volume of bonds is negligible when compared with that of cavities. It has been demonstrated that when bonds are included in porous models, the hydraulic behavior of the material can be correctly simulated [26,27]. Because drying and wetting processes evolve differently, a higher degree of saturation is obtained during drying for the same value of suction.

PSDs may be expressed in the frequency or the volumetric domain. We propose that experimental PSDs, in the frequency domain, can be approximated by a logarithmic normal distribution function where the mean size μ and the standard deviation σ are the only parameters needed to fully describe this distribution. This is called frequency distribution $f_i(\mu,\sigma)$. A single site or bond will be called element. Hence, the ith frequency will result from dividing the total number of elements

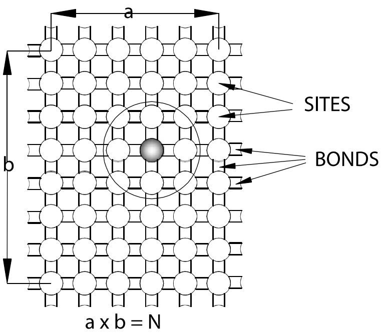

Fig. 5. Construction of the rectangular grid.

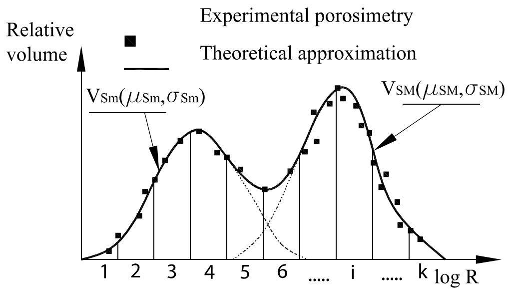

Fig. 6. Experimental (black squares) and theoretical (solid line) relative volume distributions.

n_i of the ith size by the total number of elements N. This proposal is a key feature of the model, which turns into simplicity. In a bi-dimensional porous network, cavities are represented by circles. In such a case, the ith relative volume of sites V_{Ri} results from dividing the total volume of elements of a certain size by the total volume of all elements [12,28], in the form:

$$V_{Ri} = \frac{R_i^2 f_i(\mu, \sigma)}{\sum_{i=1}^{i=k} R_i^2 f_i(\mu, \sigma)} \tag{1}$$

where k is the number of size intervals in which the entire range of pores is divided (see Fig. 6). We arrange three vectors containing k elements: a sorted vector R_i containing the sizes, a vector containing the $f_i(\mu, \sigma)$ and a vector containing the V_{Ri} distribution obtained through Eq. (1). An example of the plot of R_i versus V_{Ri} is shown in Fig. 6 where the first letter of the subscripts denotes sites S and the second one denotes macro- or micropores, M or m, respectively. It is important to highlight that these vectors should be computed for both types of pores (sites and bonds).

The procedure to build a bidimensional porous structure of a soil is as follows. We choose at random one of the n_i elements to place in the grid. Then the coordinates of the position of this element on the grid are also chosen at random. Because soils are extremely complex structures, randomness is of paramount importance; however, some limitations must be brought as we build the porous network to make it physically possible. Rojas et al. [27] propose the following geometrical constraint in order to avoid the overlap of two concurrent bonds that meet at 90° in a site:

$$R_{st} \geq \sqrt{R_{b1}^2 + R_{b2}^2} \tag{2}$$

where R_{b1} and R_{b2} are the radius of two adjacent bonds connecting to a site with radius R_{st} (Fig. 7). The condition established by Eq. (2) also ensures that bonds are always smaller than the sites they connect. Those elements that do not comply with Eq. (2) are redistributed in the network until all nodes satisfy the geometrical constraint.

When the size distributions of sites and bonds overlap, a phenomenon of segregation appears where different zones with large, medium and small pores can be found in the model. This phenomenon allows simulating the structure of real soils where small particles gather naturally forming aggregates.

The number of elements n_i of each size can be obtained with the relationship $n_i = f_i \times N$, where N is the total number of nodes in the grid.

3.2. Boundary curves

Once the network has been built, wetting and drying processes can be simulated and the SWCCs can be built. The wetting process is simulated, starting with a completely air-filled grid where suction is reduced by steps. The smallest pores

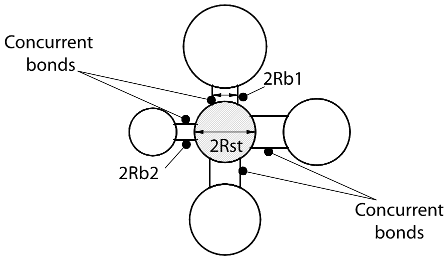

Fig. 7. Construction principle.

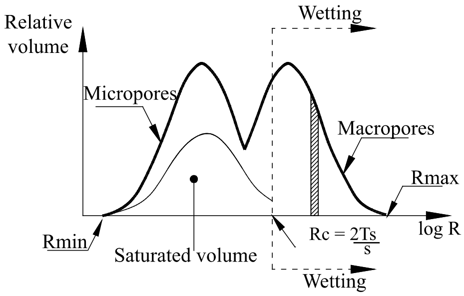

Fig. 8. Wetting process seen on a V_R distribution.

are the first to fill with water. At certain point, the limit in the size of pores that can be saturated is given by the critical radius as shown in Fig. 8. This position is called here wetting front.

Bonds can saturate when the following two conditions are fulfilled: (a) at least one of its connected sites is already filled with water and (b) its radius is smaller or equal to the critical size *Rc* obtained from the Laplace equation. Boundary bonds only need to comply with the second condition as one of their ends is directly connected to the bulk of water. Similarly, the conditions for a site to saturate are: (a) at least one of its connected bonds must be filled with water and (b) its radius must be smaller than or equal to *Rc*.

At each decrement of suction, all entities are tested to fulfill the two conditions. If a bond does, it becomes “water-activated” and its connected sites are analyzed searching for further activations. When a site is activated, automatically all of their connected bonds are activated as they are always smaller than the site. The process stops when no other element can be activated, then a new suction decrement is applied.

For each decrement on the value of suction, the wetting front indicates which bonds and sites can saturate. Observe in Fig. 8 that only a fraction of the volume behind the wetting front is saturated. This implies that not all sites that are able to saturate in the network comply with the first of the two conditions stated before. If no bubbles are trapped and all pores are connected, eventually all bonds and cavities reach the water-filled condition. The degree of saturation is computed as the current amount of water invading the pores divided by the total volume of voids:

$$S_r = V_w / V_v \tag{3}$$

During the drying process, the drying front moves from right to left. Initially, all pores in the network are filled with water, suction is nil and the drying front is placed at R_{max}. A site can dry if it complies with the two following conditions: a) at least one bond connected with the considered site is already dry, b) its radius is equal or larger than the critical size defined by the drying front. Similarly, a bond can dry if it complies with the following conditions: a) at least one of its two connected sites is already dry, and b) its radius is larger than the radius defined by the drying front. When a bond dries, automatically all of their connected sites also dry because the latter are always larger than the former.

3.3. Scanning curves

Scanning curves are intermediate processes carried out when a wetting or drying path is inverted before reaching R_{max} or R_{min}. Consider for example a drying front moving from R_{max} towards R_{min} and stopping at R_{inv} where a wetting process initiates (see Fig. 9). At this point, the dark area represents the saturated pores while the white area below the curve represents the dried pores. Therefore, only the dried pores will be able to saturate during the wetting process. After the inversion, the procedure to determine the pores that saturate proceeds exactly as in a regular wetting process where only the dry entities in the grid are tested to fulfill the conditions to be filled with water. In this way, when the degree of saturation is computed, it naturally converges towards the boundary curve. It may occur that during drying, a cluster of saturated pores forms because they are surrounded by smaller pores that require larger suction levels to dry. This is the well-known ink-bottle effect for porous media [1], which can be correctly simulated by the proposed model.

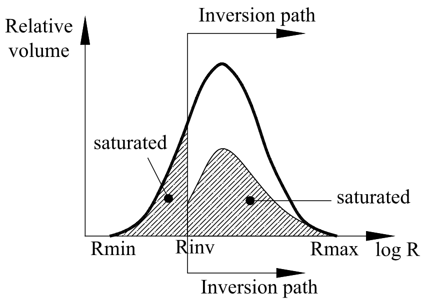

Fig. 9. Inversion process towards wetting.

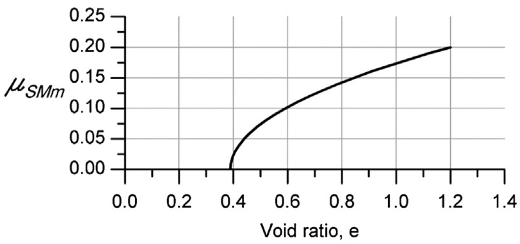

Fig. 10. Calibration curve computed from initial PSD.

3.4. Volume change

For double structured soils, two relative volume normal distributions are needed to simulate their internal structure. These distributions are $V_{\mathrm{Sm}}(\mu_{\mathrm{Sm}}, \sigma_{\mathrm{Sm}})$ and $V_{\mathrm{SM}}(\mu_{\mathrm{SM}}, \sigma_{\mathrm{SM}})$ for the case of intra-pores (micropores) and inter-pores (macropores), respectively. In this way, the final distribution can be expressed as:

$$V_{\mathrm{RS}} = g(\mu_{\mathrm{Sm}}, \sigma_{\mathrm{Sm}}, \mu_{\mathrm{SM}}, \sigma_{\mathrm{SM}}) \tag{4}$$

The procedure to determine g in Eq. (4) will be described in the next section. As stated before, it is considered here that during volumetric deformations, macropores shrink to smaller sizes. Some experimental observations indicate that the relative volume distribution of macropores displaces to the left-hand side, implying that their mean size reduces.

3.5. Model implementation

The void ratio can be obtained by adding the volume of all pore sizes when it is considered that the volume of solids is unit. Then, according to Fig. 6 and considering Eq. (1) for a bidimensional porous network, the void ratio e of the sample at certain point of the deformation can be expressed as follows:

$$e = e_{\mathrm{M}} + e_{\mathrm{m}} = fa \cdot \pi \sum_{i=1}^{k} \left\langle R_i^2 \cdot f_i(\mu_{\mathrm{SM}}, \sigma_{\mathrm{SM}}) \cdot Fpv + R_i^2 \cdot f_i(\mu_{\mathrm{Sm}}, \sigma_{\mathrm{Sm}}) \right\rangle = fa \cdot e_0 \tag{5}$$

where e_{m} and e_{M} are the total volumes of the micro and macroporosity respectively, f_i is the initial ith value of the normal frequency distribution function, R_i is the corresponding pore radius, e_0 is the void ratio of the sample at the beginning of the simulation. Parameter Fpv represents a relative volume factor that reduces the total volume of macropores to make it consistent with the volume of micropores and the void ratio of the sample. Factor fa allows retrieving the void ratio of the deformed sample and is given by:

$$fa = \frac{e}{\pi \sum_{i=1}^{k} \langle R_i^2 \cdot f_i(\mu_{\mathrm{SM}}, \sigma_{\mathrm{SM}}) \cdot Fpv + R_i^2 \cdot f_i(\mu_{\mathrm{Sm}}, \sigma_{\mathrm{Sm}}) \rangle} \tag{6}$$

The model considers that volume strains are due solely to the shrinkage of macropores. Then if all parameters of the pore size distribution are kept constant except the mean size of macropores μ_{SM}, Eq. (5) can be written as a function of μ_{SM}. This equation has been plotted in Fig. 10 and can be used to determine the exact value for parameter μ_{SM} such that the distribution of the relative volume of sites V_{RS} retrieves the required void ratio.

The total volume of micropores e_{m} and macropores e_{M} shown in Fig. 10 are 0.39 and 0.81, respectively, representing a void ratio of 1.2. This figure shows how the void ratio reduces with parameter μ_{SM}. Eventually, the sample may reach a point where macropores almost completely disappear ($\mu_{\mathrm{SM}} = 0.05$), while the void ratio remains practically unchanged with further reduction of parameter μ_{SM}. This point may correspond to the contraction limit of the material.

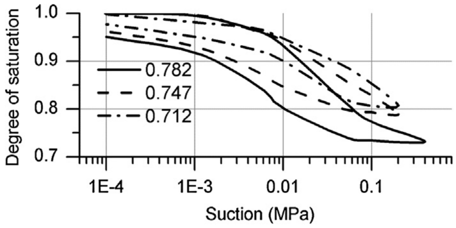

Fig. 11. Drying–wetting cycles of a compacted volcanic soil.

Table 1
Parameters used to reproduce the SWCCs of a volcanic soil.

μ_{SM}	σ_{SM}	μ_{Sm}	σ_{Sm}	μ_{BM}	σ_{BM}	μ_{Bm}	σ_{Bm}
0.010	7.000	0.001	4.000	0.500	6.000	0.001	5.000

Finally, the relative volume distribution for each void ratio can be obtained with the new mean size of macropores μ_{SMm} obtained from the calibration curve (Eq. (7)):

$$V_{RSi} = \frac{(R_i^2 \cdot f_i(\mu_{SMm}, \sigma_{SM}) \cdot Fpv + R_i^2 \cdot f_i(\mu_{Sm}, \sigma_{Sm}))}{\sum_{i=1}^{i=k}(R_i^2 \cdot f_i(\mu_{SMm}, \sigma_{SM}) \cdot Fpv) + \sum_{i=1}^{i=k}(R_i^2 \cdot f_i(\mu_{Sm}, \sigma_{Sm}))} \tag{7}$$

Each time that the void ratio of the sample changes, the new SWCCs can be determined with the procedure outlined above. When the material is deforming due to suction increase, every single point of the SWCC has to be recalculated by reinitiating the simulation from the initial point of the curve or from the inversion point when wetting–drying cycles are being applied. This is so because the PSD modifies itself for each increment of suction and therefore the volume of intruded water in the deformed pores also changes. This process continues till the end of the test.

For each increment or decrement of suction, the degree of saturation is computed using Eq. (3) and the SWCC in drying or wetting can be plotted. The size of the network used for these particular simulations was 1000 × 1000 elements. It is worth mentioning that further simulations with larger grids have shown that the size of the network does not influence the results when it is made of at least 1000 × 1000 elements.

4. Numerical and experimental comparisons

4.1. Volcanic soil

Ng and Pang [29] prepared compacted soil samples from a soil mixture containing 4.9, 20.1, 36.6 and 37.1% of gravel, sand, silt and clay, respectively. This soil is classified as high-plasticity sandy silt clay. Three samples were statically compacted to different densities in an oedometer ring and their SWCCs during drying–wetting cycles were obtained using pressure extractors (see Fig. 11). The initial void ratios for each sample were 0.782, 0.747 and 0.712, respectively.

The initial PSD parameters for the porous model were obtained by simulating the drying–wetting cycle of the sample compacted at a void ratio of 0.782. The resulting parameters are depicted in Table 1. Relative volume factors of 0.00008 and 0.00145 for macropores and larger bonds were used respectively. Using Eq. (6) factor $fa = 218.84$ is found for $e = 0.782$. The number of divisions in which the relative volume distribution has been discretized was $k = 200$ (see Fig. 6). As explained earlier, it is assumed that only macropores shift to smaller sizes, hence, parameters σ_{SM}, μ_{Sm}, σ_{Sm}, μ_{BM}, σ_{BM}, μ_{Bm} and σ_{Bm} remain constant when simulating the SWCCs for void ratios 0.747 and 0.712.

Fig. 12 compares model predictions and experimental measurements. Predicted PSDs are also shown in Fig. 12d. Observe that the proposed model adequately simulates the evolution of the SWCCs with the volumetric deformation.

4.2. Pearl clay

Sun et al. [30] obtained the SWCC during wetting–drying cycles of samples containing 50% of silt and 50% of clay called Pearl clay. The liquid limit and the plastic indexes for this material are 49% and 22%, respectively. The soil can be classified as clay of low compressibility according to the Unified Soil Classification System. Two statically compacted samples were prepared at initial void ratios of 1.08 and 1.78 to obtain their SWCCs. The specimens, 3.5 cm in height and 3.5 cm in diameter, were tested in a suction controlled triaxial cell. Volumetric strains were measured during the entire wetting–drying cycle. Fig. 13 depicts the experimental SWCCs of a sample tested at an initial void ratio of 1.088 corresponding to a degree of saturation of 58.5% (point A). Then the sample was subjected to wetting–drying cycles.

In order to find out the parameters of the model at the initial conditions, the experimental points of the first wetting (path AB) were used. This is so because no important volume change occurs during this cycle (path AB). In addition, at the end of compaction, the state of the sample is close to that on the main drying retention curve. This consideration

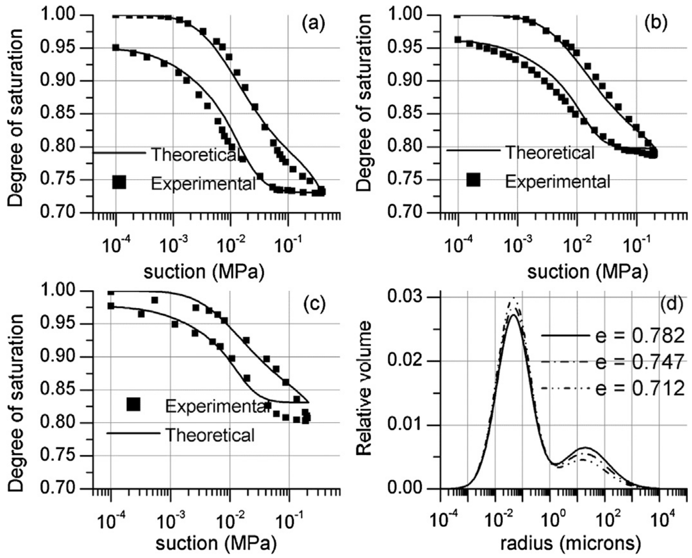

Fig. 12. Simulations of SWCCs. (a) Best fit for sample with $e = 0.782$. Experimental and numerical results for (b) $e = 0.747$ and (c) $e = 0.712$ and (d) evolution of the relative volume with void ratio. Experimental results by Ng and Pang [29].

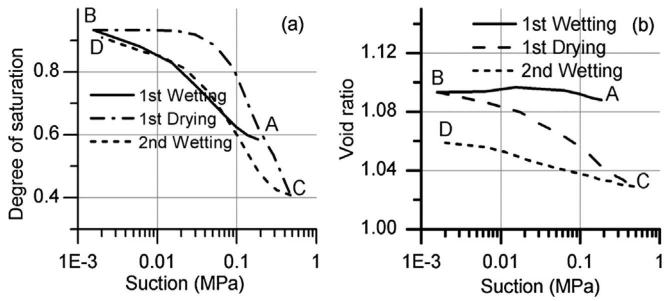

Fig. 13. (a) Experimental SWCCs for sample compacted at $e = 1.08$ and (b) volume change characteristics. Experimental data by Sun et al. [30].

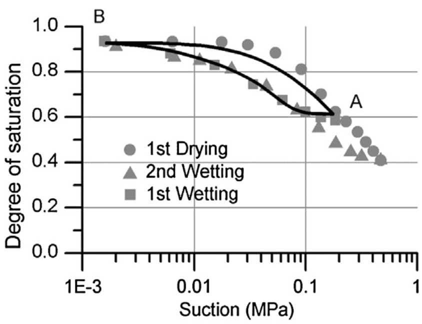

Fig. 14. Procedure to obtain the unsaturated state of the network for sample 1.

comes from the fact that, when samples are being statically compacted, their degree of saturation increases. Then, when the stress is released, a small relaxation occurs and consequently the degree of saturation decreases. Therefore, at the end of compaction, the soil sample lies close to the drying curve, although most probably not exactly on it. Then, the simulation to obtain the initial parameters of the soil starts at point B in Fig. 14, then reaches point A and comes back to point B. The parameters resulting from this simulation are shown in Table 2. Relative volume factors of 0.02 and 0.001 were used for macropores and larger bonds, respectively.

Once the parameters of the model have been obtained, it is possible to simulate the entire wetting–drying path, including the effect of volumetric deformation (Fig. 15a). The PSD of the material was updated for each increment of suction till the end of the test.

Table 2
Model parameters for soil sample compacted at $e = 1.08$.

μ_{SM}	σ_{SM}	μ_{Sm}	σ_{Sm}	μ_{BM}	σ_{BM}	μ_{Bm}	σ_{Bm}
0.2	4.0	0.04	3.0	0.1	3.58	0.001	10.0

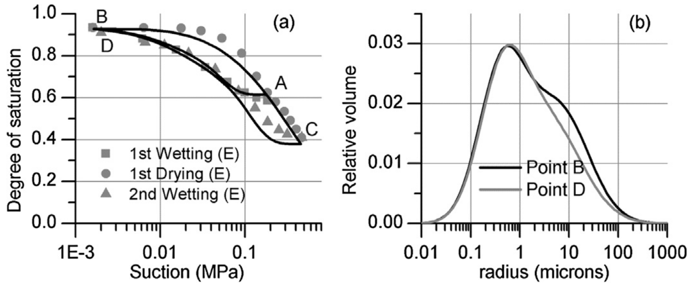

Fig. 15. (a) Numerical (solid line) and experimental (E) predictions on the SWCC and (b) relative volume distribution evolution.

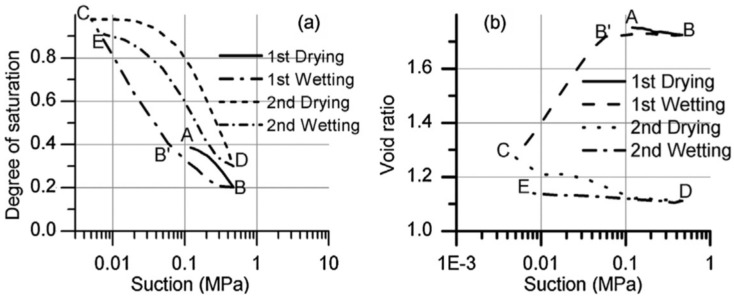

Fig. 16. (a) Experimental SWCCs for sample compacted at $e = 1.78$ and (b) volume change characteristics. Experimental data by Sun et al. [30].

Fig. 15b shows the PSD for points B and D. It can be observed that the evolution of this curve is rather small, because the change in the void ratio during the test is also small, as shown in Fig. 13b.

Another sample was compacted at an initial void ratio of 1.78 and subjected to wetting–drying cycles while the volumetric deformation was recorded. Fig. 16a shows the shift of the retention curve with suction, while Fig. 16b shows the volumetric strains of the sample during the test. A small drying process was initially carried out from point A to point B. Then the sample was subject to three large wetting–drying semi-cycles. Observe that even if most of the volumetric deformation of the soil occurs during the initial wetting path BC, most of the shifting of the retention curve occurs later. This volumetric reduction indicates that macropores are collapsing during wetting. In contrast, no appreciable volume change occurs following paths AB and DE.

The same procedure used before to determine the initial model parameters is applied here. The initial part of the first drying (path AB) can be considered as a portion of a scanning curve. This is so because, as aforementioned, at the end of compaction the soil sample lies close to the main drying curve, although most probably not exactly on it. After a small increment of suction, the main drying curve is reached. Also observe in Fig. 16b that during the small cycle ABB', the soil practically does not show any volumetric change. Then, it can be considered that, excluding the initial part of path AB, the experimental points of the path ABB' represent a small cycle of the initial SWCCs of the material. By fitting the numerical with the experimental retention curves along this path (Fig. 17), the initial parameters of the porous model can be obtained. These parameters are shown in Table 3. Relative volume factors of 0.02 and 0.001 were used for macropores and for the larger bonds, respectively. Using Eq. (6), a factor $fa = 0.60$ was found for the initial void ratio. Note that the fitting procedure provides the same parameters for both Pearl Clay samples. This is consistent, since both samples were built up from the same type of soil at the same water content.

Once the initial parameters of the model have been obtained, it is possible to simulate the shift of the retention curve with volumetric deformation. Fig. 18a shows this shifting following the full drying–wetting path. Fig. 18b depicts the relative volume distribution at the initial conditions (point B) and at the end of the last wetting cycle (point E in the same figure). Notice that this sample exhibits a clear change in the relative volume distribution of macropores when compared with the results of the previous sample (Fig. 15b). This is due to the small volumetric deformation observed in the last case. Also notice that numerical simulations follow quite accurately the shift of the retention curve. It is worth noting that model parameters are kept the same for both samples ($e = 1.08$ and $e = 1.78$).

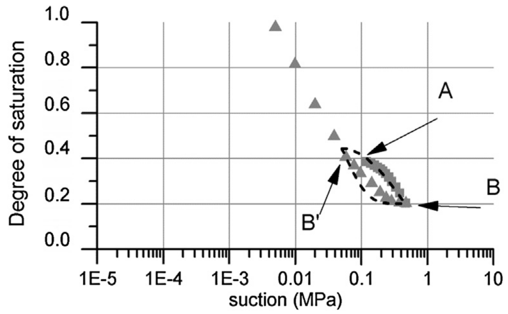

Fig. 17. Procedure to approximate the initial network for point A.

Table 3
Model parameters for soil sample compacted at $e = 1.78$.

μ_{SM}	σ_{SM}	μ_{Sm}	σ_{Sm}	μ_{Bm}	σ_{Bm}	μ_{BM}	σ_{BM}
0.2	4.0	0.04	3.0	0.1	3.58	0.001	10.0

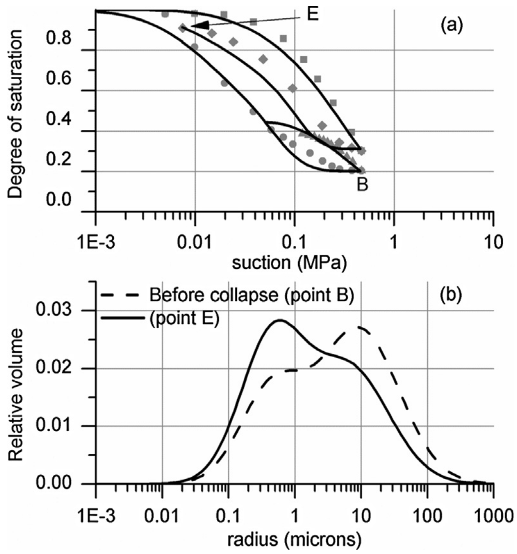

Fig. 18. (a) Numerical (solid line) and experimental (scattered lines) result comparisons of SWCCs, and (b) PSD evolution through path BC.

5. Conclusions

A model to predict the evolution of the SWCCs of soils based on the volumetric deformations has been presented herein. The SWCC during wetting–drying cycles is obtained by simulating intrusion and drainage of water in the porous structure of the material. The porous structure of the soil was modeled as a bidimensional network built with entities such as sites and bonds. By fitting the numerical with the experimental SWCCs, the pore size distribution of the soil can be obtained. This pore-size distribution is used to define the number of entities of each size.

The shift of the SWCCs with the volumetric deformation of the soil is modeled by doing a simple assumption: the reduction of the mean size of macropores in the network occurs homogeneously when an increment of the mean stress or suction is applied. With this assumption, the proposed porous model is able to simulate quite precisely the shift of the SWCCs with volumetric deformations produced by collapse upon wetting, loading or drying. This paper shows that reducing homogeneously the mean size of the macropores is sufficient to correctly describe the deformation mechanism of double-porosity media.

Acknowledgements

This project was funded by the Consejo Nacional de Ciencia y Tecnología (CONACyT) in Mexico through grant number 349586/238050. Their support is greatly acknowledged.

References

[1] N. Lu, W.J. Likos, Unsaturated Soil Mechanics, John Wiley & Sons, New York, 2004.
[2] A. Gens, M. Sánchez, D. Sheng, On constitutive modelling of unsaturated soils, Acta Geotech. 1 (2006).
[3] G.T. Houlsby, The work input to an unsaturated granular material, Geotechnique 47 (1997) 193–196.
[4] R. Brooks, A. Corey, Hydraulic properties of porous media, Hydrol. Pap., Colo. State Univ. (1964) 1–24.
[5] N. Khalili, M.A. Habte, S. Zargarbashi, A fully coupled flow deformation model for cyclic analysis of unsaturated soils including hydraulic and mechanical hysteresis, Comput. Geotech. 35 (2008) 872–889.
[6] A. Assouline, Modeling the relationship between soil bulk density and the water retention curve, Vadose Zone J. 5 (2006) 554–563.
[7] D. Gallipoli, A hysteretic soil-water retention model accounting for cyclic variations of suction and void ratio, Geotechnique 62 (2012) 605–616.
[8] E. Romero, J. Vaunat, Retention curves of deformable clays, in: Proceedings of the International Workshop on Unsaturated Soils, Trento, Italy, 2000.
[9] J. Vaunat, E. Romero, C. Jommi, An elastoplastic hydro-mechanical model for unsaturated soils, in: A.E. Tarantino, C. Mancuso, C.E. Mancuso (Eds.), Experimental Evidence and Theoretical Approaches in Unsaturated Soils, A.A. Balkema, Trento, Italy, 2000.
[10] M.T. van Genutchen, A closed form equation of predicting the hydraulic conductivity of unsaturated soils, Soil Sci. Soc. Am. J. 44 (1980) 892–898.
[11] A. Koliji, L. Laloui, O. Cuisinier, L. Vulliet, Suction induced effects on the fabric of a structured soil, Transp. Porous Media 64 (2006) 261–278.
[12] H. Arroyo, E. Rojas, M.L. Pérez-Rea, J. Horta, J. Arroyo, Simulation of the shear strength for unsaturated soils, C. R. Mecanique 341 (2013) 727–742.
[13] E. Rojas, M.L. Pérez-Rea, G. Gallegos, J. Leal, A porous model for the interpretation of mercury porosimetry tests, J. Porous Media 15 (2012) 517–530.
[14] P. Delage, M. Audiguier, Y.J. Cui, M.D. Howat, Microstructure of a compacted silt, Can. Geotech. J. 33 (1996) 150–158.
[15] P.H. Simms, E.K. Yanful, A pore-network model for hydro-mechanical coupling in unsaturated compacted clayey soils, Can. Geotech. J. 42 (2005) 499–514.
[16] E. Romero, C. Hoffmann, E. Castellanos, J. Suriol, A. Lloret, Microstructural changes of compacted bentonite induced by hydro-mechanical actions, in: E.E. Alonso, A. Ledesma (Eds.), Advances in Understanding Engineered Clay Barriers, Balkema, Rotterdam, The Netherlands, 2005.
[17] O. Cuisinier, L. Laloui, Fabric evolution during hydromechanical loading of a compacted silt, Int. J. Numer. Anal. Methods Geomech. 28 (2004) 483–499.
[18] A.E. Tarantino, E. De Col, Compaction behaviour of clay, Geotechnique 58 (2008) 199–213.
[19] P.H. Simms, E.K. Yanful, Measurement and estimation of pore shrinkage and pore distribution in a clayey till during soil–water characteristic curve tests, Can. Geotech. J. 38 (2001) 741–754.
[20] J.J.M. van der Meer, J. Menzies, J. Rose, Subglacial till: the deforming glacier bed, Quat. Sci. Rev. 22 (2003) 1659–1685.
[21] L. Barden, A. McGown, K. Collins, The collapse mechanism in partly saturated soil, Eng. Geol. 7 (1973) 49–60.
[22] A. El Howayek, P. Huang, R. Bisnett, M.C. Santagata, Identification and behavior of collapsible soils, Joint Transportation Research Program, 2011.
[23] D.P. Coduto, Foundation Design, Principles and Practices, Prentice Hall, Upper Saddle River, NJ, USA, 1994.
[24] Y.J. Cui, C. Loiseau, P. Delage, Microstructure changes of a confined swelling soil due to suction controlled hydration, in: J.F.T. Jucá, T.M.P.d. Campos, F.A.M. Marinho (Eds.), Unsaturated Soils, Balkema, Leiden, The Netherlands, 2002.
[25] R. Thom, R. Sivakumar, V. Sivakumar, E.J. Murray, P. Mackinnon, Pore size distribution of unsaturated compacted kaolin: the initial states and final states following saturation, Geotechnique 57 (2007) 469–474.
[26] J. Horta, E. Rojas, M.L. Pérez-Rea, T. López, J.B. Zaragoza, A random solid–porous model to simulate the retention curves of soils, Int. J. Numer. Anal. Methods Geomech. 37 (2013).
[27] E. Rojas, A.G. Zepeda, M.L. Pérez-Rea, J. Leal, G. Gallegos, A four elements porous model to estimate the strength of unsaturated soils, Geotech. Geolog. Eng. 29 (2009) 193–202.
[28] E. Rojas, J. Horta, T. López-Lara, J.B. Hernández, A probabilistic solid porous model to determine the shear strength of unsaturated soils, Probab. Eng. Mech. 26 (2011).
[29] C.W.W. Ng, Y.W. Pang, Experimental investigations of the soil-water characteristics of a volcanic soil, Can. Geotech. J. 37 (2000) 1252–1264.
[30] D.A. Sun, D.C. Sheng, H.B. Cui, S.W. Sloan, A density-dependent elastoplastic hydro-mechanical model for unsaturated compacted soils, Int. J. Numer. Anal. Methods Geomech. 31 (2007) 1257–1279.